Front. Environ. Sci. Eng. 2020, 14(6): 107
https://doi.org/10.1007/s11783-020-1286-1

RESEARCH ARTICLE

# Cross-stacked super-aligned carbon nanotube/activated carbon composite electrodes for efficient water purification via capacitive deionization enhanced ultrafiltration

**Min Li[1], Shuai Liang (✉)[1], Yang Wu[2], Meiyue Yang[1], Xia Huang (✉)[3]**

1 Beijing Key Laboratory for Source Control Technology of Water Pollution, College of Environmental Science and Engineering, Beijing Forestry University, Beijing 100083, China

2 Department of Mechanical Engineering and Tsinghua Foxconn Nanotechnology Research Center, Tsinghua University, Beijing 100084, China

3 State Key Joint Laboratory of Environment Simulation and Pollution Control, School of Environment, Tsinghua University, Beijing 100084, China

## HIGHLIGHTS

- A high-performance electrode was prepared with super-aligned carbon nanotubes.
- SACNT/AC electrode achieved a ~100% increase in desalination capacity and rate.
- SACNT/AC electrode achieved a ~26% increase in charge efficiency.
- CUF process with SACNT/AC achieved an up to 2.43-fold fouling reduction.
- SACNT/AC imparts overall improved water purification efficiency.

## GRAPHIC ABSTRACT

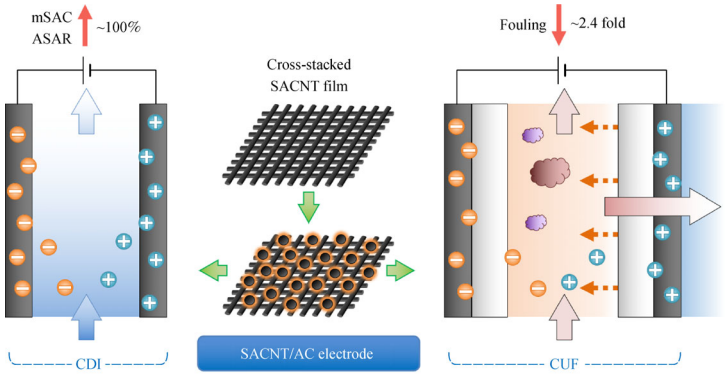


## ARTICLE INFO

*Article history:*
Received 28 April 2020
Revised 21 May 2020
Accepted 25 May 2020
Available online 29 June 2020

*Keywords:*
Carbon nanotube
Super aligned
Conductive membrane
Capacitive deionization
Ultrafiltration
Desalination

## ABSTRACT

The practical application of the capacitive deionization (CDI) enhanced ultrafiltration (CUF) technology is hampered due to low performance of electrodes. The current study demonstrated a novel super-aligned carbon nanotube (SACNT)/activated carbon (AC) composite electrode, which was prepared through coating AC on a cross-stacked SACNT film. The desalination capability and water purification performance of the prepared electrode were systematically investigated at different applied voltages (0.8–1.2 V) with a CDI system and a CUF system, respectively. In the CDI tests, as compared with the control AC electrode, the SACNT/AC electrode achieved an approximately 100% increase in both maximum salt adsorption capacity and average salt adsorption rate under all the applied voltage conditions, demonstrating a superior desalination capability. Meanwhile, a conspicuous increase by an average of ~26% in charge efficiency was also achieved at all the voltages. In the CUF tests, as compared with the control run at 0 V, the treatment runs at 0.8, 1.0, and 1.2 V achieved a 2.40-fold, 2.08-fold, and 2.43-fold reduction in membrane fouling (calculated according to the final transmembrane pressure (TMP) data at the end of every purification stage), respectively. The average TMP increasing rates at 0.8, 1.0, and 1.2 V were also roughly two times smaller than that at 0 V, indicating a dramatical reduction of membrane fouling. The SACNT/AC electrode also maintained its superior desalination capability in the CUF process, resulting in an overall improved water purification efficiency.



## 1 Introduction

To meet the growing global water demand for life and production, effective strategies and efficient water treatment technologies which aim to augment water resources are in urgent need (Mekonnen and Hoekstra, 2016).

✉ Corresponding authors
E-mail: shuai_liang@bjfu.edu.cn (S. Liang);
xhuang@tsinghua.edu.cn (X. Huang)

Membrane separation technology, owing to its advantages such as reliable permeate quality, small footprint, and so forth, has achieved tremendous development in practical applications (Xiao et al., 2019; Zhu et al., 2019). The rapid advances in related fields such as wastewater reclamation and seawater desalination also bring promising prospects in lifting the water crisis (Caldera and Breyer, 2017; Ma et al., 2018; Tay et al., 2018). However, while most developed cities and towns have built complete centralized water treatment facilities, the water problems in many remote and underdeveloped areas are still less concerned (Omosa et al., 2012; Mekonnen and Hoekstra, 2016). Besides, the conventional centralized treatment processes are not suitable for use in those areas for their lack of stable drainage and continuous wastewater treatment demands (Jung et al., 2018). Therefore, it is of great significance to develop highly efficient decentralized water treatment technologies (Lu et al., 2019; Liu et al., 2020).

Membrane separation is one of the most promising technologies for decentralized applications. Nevertheless, the ubiquitous membrane fouling problem and high energy consumption issue reduce its sustainability in engineering applications (Kamali et al., 2019). Effective approaches to the alleviation of membrane fouling have been developed with tremendous efforts from various perspectives, including antifouling materials (Liang et al., 2018; Zhao et al., 2018; Guo et al., 2019), hybrid operations (Liang et al., 2014; Zhao et al., 2019), design optimization (Yan et al., 2015; Wang and Lin, 2019), and so on. Among them, the electrofiltration strategy, which incorporates the electrical power in the filtration process with conductive membranes or external electrodes, has been widely recognized as efficient and sustainable in mitigating membrane fouling (Wang et al., 2015; Zhu et al., 2018; Hu et al., 2019). Besides, there is a growing demand for desalination in the wastewater treatment filed (Liang et al., 2019) due to increasingly stringent effluent quality standards. In such an application scenario, a complete desalination is often not required while a moderate salinity decrease will be sufficient to fulfill the effluent standard. Therefore, the conventional high-pressure desalination technology (e.g., nanofiltration and reverse osmosis) which possesses superior rejection capability is over-qualified for such applications. Capacitive deionization (CDI), as an emerging desalination technology, has been widely reported as a potential efficient technology in desalinating low-salinity water (Suss et al., 2015; Choi et al., 2019). Although its limitations compared with the dominating desalination technologies such as reverse osmosis have been reported recently (Lin, 2020; Patel et al., 2020), the ceaseless development of these kinds of new technologies still provides rich possibilities for the development of highly efficient and sustainable water purification processes.

Recently, we developed a novel CDI enhanced ultrafiltration (CUF) process (Liang et al., 2019) through incorporating a CDI module into a UF unit. The established CUF system combined the advantageous characteristics of both the electrofiltration and CDI technologies, and achieved a simultaneous removal of foulants and salts. The inherent electrical power from CDI led to a conspicuous reduction of membrane fouling owing to an electric field based foulant-repulsion effect. The existence of the UF membranes facilitated the desalination process through, for example, protecting the electrode from fouling. As a whole, the CUF process achieved an overall improved treatment efficiency. However, the further application of the CUF process is still hampered with several challenges. One big challenge is the low desalination capacity of the electrodes. The widely used electrodes for electrosorption are mainly made of activated carbon (AC) (Li et al., 2020). But most of them are not suitable for the CUF application. To be appropriately incorporated with the ultrafiltration (UF) membrane, the electrodes for the CUF process should be highly flexible, permeable, thin, and sufficiently strong. Super-aligned carbon nanotube (SACNT), as a highly ordered and flexible nanomaterial with an ultrahigh specific surface area (Liu et al., 2008), possesses the potential advantage of being made into high-performance flow-through electrodes. However, relevant research on the application of SACNT in water treatment has rarely been reported. Besides, the configuration, architecture, and operating conditions of the CUF system also need to be further improved to exploit the capability of the electrode.

In view of the above, the current study prepared a novel SACNT/AC composite electrode by coating AC on a cross-stacked SACNT film. The desalination and integrated water purification performance of the prepared electrode was systematically investigated with a CDI system and a newly designed CUF system, respectively. A series of CDI and CUF experiments were performed at different applied voltages (ranging from 0.8 to 1.2 V) with different synthetic solutions. On the basis of systematical tests and calculations, the overall treatment performance of the SACNT/AC electrode was evaluated.

## 2 Materials and methods

### 2.1 Preparation of SACNT/AC electrode

Prior to prepare the SACNT/AC electrode, a cross-stacked SACNT film comprising 200 SACNT layers was fabricated on the basis of a previously reported method (Zhang et al., 2006; Liu et al., 2011). As illustrated in Fig. 1, the layers of SACNT array each contained numerous parallel-aligned SACNT yarns were sequentially stacked on a non-woven polyethylene terephthalate (PET) fabric (Ahlstrom-Munksjö, Finland) in orthogonal directions. After being immersed in ethanal for 30 min for densification, the resultant cross-stacked SACNT framework gained

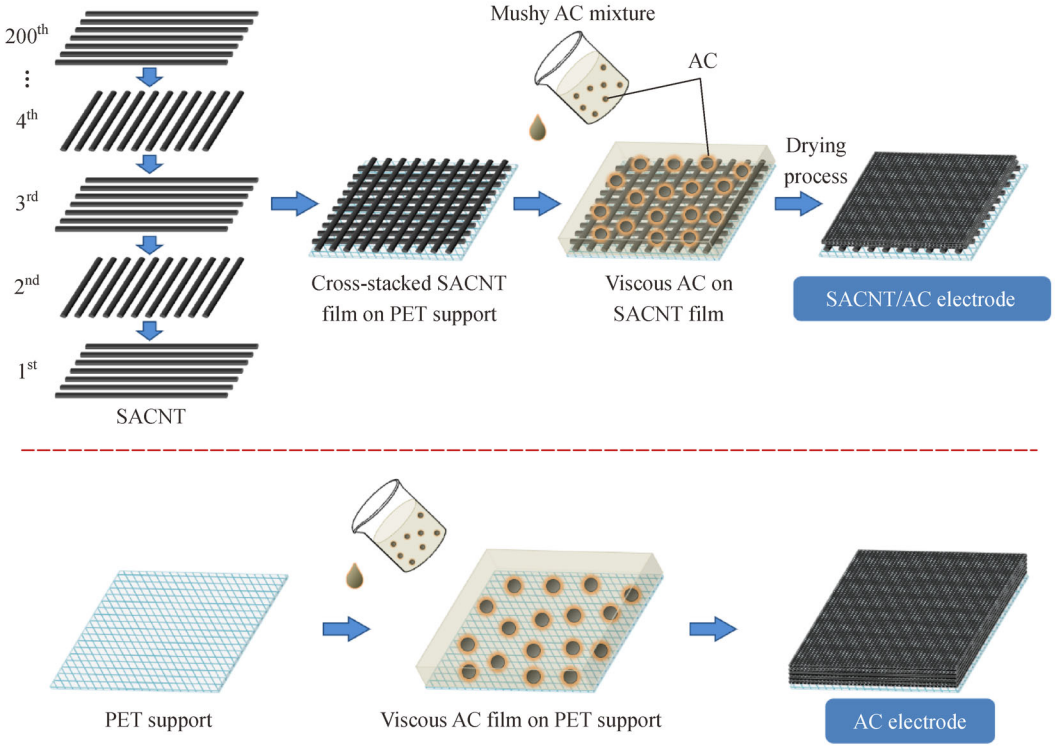


**Fig. 1** Schematic diagram illustrating the fabrication processes of the super-aligned carbon nanotube (SACNT) / activated carbon (AC) composite electrode and AC electrode (served as a control).

sufficient mechanical strength owing to internal Van der Waals interactions between the CNTs (Liu et al., 2011). The obtained free-standing SACNT film was then air-dried and stocked at room temperature (23 ± 1°C) prior to use. Afterwards, a mushy AC mixture was prepared through blending 8 g of AC powder (YEC-200D, Yihuan Carbon, China), 1 g of acetylene black (BC-90, Tianjin Baochi, China), and 1 g of polyvinylidene fluoride (PVDF, Solef 6010, Belgium) with 40 g of *N*-Methyl-2-pyrrolidinone (NMP, anhydrous, 99.5%, Sigma–Aldrich) under vigorous stirring. After 24 h, a ~0.15 g portion of the resulted AC mixture was evenly applied to the surface of the cross-stacked SACNT film on the PET support. After dried at 50°C for 1 h, the obtained SACNT/AC electrode was stored in a 4°C DI water bath prior to further tests. For comparative research, a control AC electrode was prepared by casting ~0.16 g of AC mixture directly on the PET support. The applied extra 0.01 g of AC was meant to ensure that the final SACNT/AC and AC electrodes possessed a roughly equal mass.

## 2.2 Characterization of electrode morphology

The top surface and cross sections of the SACNT film and electrodes were observed through a field emission scanning electron microscope (FE-SEM, SU8010, Hitachi, Japan). To obtain the cross-sectional specimen, the electrode was fractured in liquid nitrogen.

## 2.3 CDI and CUF systems

A CDI system was set up to test the CDI performance of the electrodes. A CUF system was set up to assess the integrated water purification performance of the electrodes. The cell configurations of both systems were illustrated in Fig. 2. The core cell of the CDI system (Fig. 2A) included two identical electrodes (two AC or two SACNT/AC electrodes), which were oppositely placed with their functional sides (not the PET support sides) facing each other. A mesh spacer was inserted between the electrodes to prevent short circuit and also formed a 1.5 mm thick cross-flow chamber. The effective filtration area for each electrode is ~22 $cm^2$ (2 cm × 11 cm). Titanium conductors (pre-sandblasted and coated with platinum to minimize passivation) were used to connect the electrodes to an electrochemical workstation (CHI650E, CH Instruments, Inc., USA), which controlled the applied cell voltage. Silicone rubber frames were used to seal the cell and prevent leaching. The CUF cell possesses a similar configuration (Fig. 2B) with the CDI cell. The primary difference is that two PVDF UF membranes are installed between the electrodes in the CUF configuration, with the

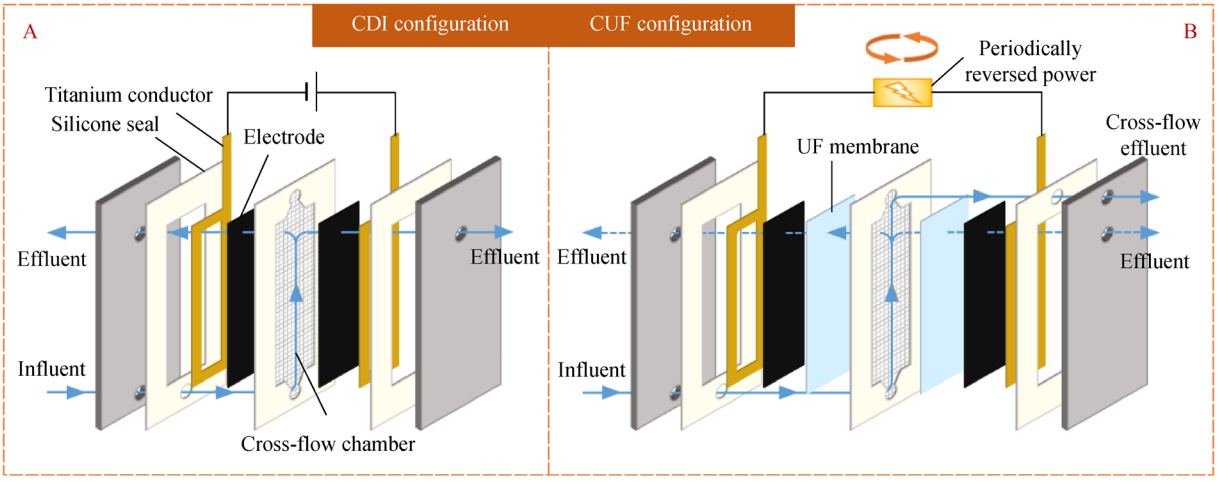


**Fig. 2** Configuration diagram of the (A) capacitive deionization (CDI) cell and (B) capacitive deionization enhanced ultrafiltration (CUF) cell.

skin layers of both membranes orienting toward the cross-flow chamber. The PVDF membranes were prepared with a non-solvent induced phase separation method (Chen et al., 2019; Ma et al., 2019). Briefly, 15 g of PVDF (Solef 6010, Belgium) and 1 g of polyvinylpyrrolidone (MW ~10 000, Sigma–Aldrich) were completely dissolved into 84 g of *N*,*N*-dimethylformamide to prepare the casting solution. After the annealing (50°C, 1 h) and degasification (12 h storage) processes, the casting solution was spread on a glass plate in a thickness of 250 μm using an applicator (Elcometer 3530, UK). Then the glass plate was transferred to a DI water bath where the membrane gradually formed through polymer coagulation.

The CDI and CUF systems were operated in different modes. The CDI system was operated in a two-side flow-through mode (Suss et al., 2015; Choi et al., 2019). Briefly, the influent (1.4 mL/min) was ceaselessly driven with peristaltic pumps (BT100-1L, Longer Pump, China) into the cross-flow chamber (Fig. 2A) and flow through the electrodes on both the anode and cathode sides. The permeate converged at the effluent outlets and flow out of the cell. The effluent on both sides were mixed prior to further measurements. The CUF system was operated in a one-side flow-through mode. Briefly, in each treatment cycle, the influent was driven through the UF membrane and electrode on the cathode side, while the anode side was closed. Besides, the power orientation would be reversed after each treatment cycle, and the membrane and electrode on the other side would be open for effluent in the next cycle (see illustration in Fig. S1 in the Supporting Information). Such an operational mode was designed to minimize the accumulation of irreversible fouling. More details were given in Section 2.5.

In addition, effluent conductivity was monitored with several conductivity meters (EPU 452, eDAQ Pty. Ltd., Australia). In the CUF system, pressure sensors (HYDZ-800, Huayang Dongzhuo Automation Equipment, China) were employed to record the variation of transmembrane pressure (TMP, i.e., the pressure difference between the influent and transmembrane effluent), which indicated the development of membrane fouling.

### 2.4 Evaluation of CDI performance of electrodes

The CDI performance of the electrode was quantified in terms of maximum salt adsorption capacity (mSAC), average salt adsorption rate (ASAR), and charge efficiency ($\Lambda$). For each electrode type, a series of multi-cycle desalination experiments were conducted in a single-pass manner (Porada et al., 2013) at different voltages (0.8, 0.9, 1.0, 1.1, and 1.2 V). Each experimental cycle contained a 60 min adsorption stage where the electrical power was applied (0.8, 0.9, 1.0, 1.1, or 1.2 V) and a 60 min desorption stage where no electrical power was applied (i.e., 0 V was applied). A 1 g/L KCl solution was used as the feed solution. The data in the last two cycles of each experimental run were used for calculations. The mSAC (mg/g) was calculated as the ratio of the maximum mass of the removed salt to the mass of the electrode pair (Suss et al., 2015). The ASAR ($R_a$, mg/(g·min)) was calculated as the ratio of the mSAC to the duration time of the adsorption stage (i.e., 60 min). Also, the salt adsorption rate (SAR) at a specific time $t$ ($R_{at}$, mg/(g·min)) was calculated with Eq. (1):

$$R_{at} = \frac{1}{n} \cdot \sum_{i=1}^{n} \frac{\phi_{ti}}{\Delta t} \tag{1}$$

where the $\phi_{ti}$ indicated the SAC (mg/g) over the 0–$t$ period in the $i$th cycle, the $\Delta t$ indicated the relative time duration (i.e., $\Delta t = t - 0$ min), and $n$ indicated the number of operational cycles ($n = 2$ in this section). The $\Lambda$ (%) was

calculated as the ratio of the quantity of adsorbed salt to the charge during adsorption in units of moles (Suss et al., 2015).

### 2.5 Evaluation of water purification performance in CUF system

The water purification performance of the electrode was characterized in terms of fouling inhibition, foulant retention, and desalination aspects with the CUF system. A synthetic wastewater was prepared as the feed solution to the system. The synthetic wastewater included 5 mg/L of bovine serum albumin (BSA, 66 kDa, Sigma–Aldrich), 10 mg/L of humic acid (HA, Aldrich), 20 mg/L of sodium alginate (SA, Aldrich), and 1 g/L of KCl. A series of six-cycle CUF experiments were performed. Each cycle comprised a 15 min purification stage where the voltage was applied (0.8, 1.0, or 1.2 V) and a 15 min discharging stage where no voltage was applied (0 V). At every purification stage, a stream was continuously driven across the UF membrane and cathode at 2 mL/min as a purified effluent. At every discharging stage, the pumps were turned off in the first 10 min, allowing the desorption of adsorbed salts and decompression of deposited foulants. In the next 5 min, the cross-flow channel was open thereby discharging the concentrated stream away from the cell.

The membrane fouling status was evaluated on the basis of the recorded TMP changes. A lower TMP and a smaller average increasing rate of the TMP ($R_p$) indicate less membrane fouling. The $R_p$ was calculated using Eq. (2):

$$R_p = \frac{1}{6} \cdot \sum_{i=1}^{6} \frac{P_{it'} - P_{i0}}{\Delta t'} \tag{2}$$

where the $P_{i0}$ and $P_{it'}$ indicated the initial and final TMPs in the $i$th cycle, respectively; and the $\Delta t'$ indicated the duration of the purification stage (i.e., 15 min). In addition, the total organic carbon (TOC) of the effluent was regularly measured (TOC-VCSH, Shimadzu, Japan), and the average foulant-retention rate ($\varphi$, %) was calculated with Eq. (3):

$$\varphi = \frac{1}{6} \cdot \sum_{i=1}^{6} \left(1 - \frac{C_{ie}}{C_0}\right) \tag{3}$$

where the $C_0$ and $C_{ie}$ indicated the averaged TOC concentration of the influent and effluent in the $i$th cycle, respectively. Moreover, on the basis of monitored effluent conductivity, the $R_{at}$ (mg/(g·min)) was also calculated using Eq. (1) with the $n = 6$ in this section.

## 3 Results and discussion

### 3.1 Morphology of SACNT/AC electrode

Figure 3 presents the morphologies of the SACNT film, AC electrode, and SACNT/AC composite electrode through the SEM view. In a relatively macro perspective (Fig. 3A), the SACNT film exhibits a smooth surface morphology with an orthogonal crossing texture. The arrows in Fig. 3A indicate the extending directions of the SACNTs. In general, the SACNT film is uniform and dense. In a relatively micro perspective (Fig. 3B), the cross-stacked morphology composed of orderly aligned SACNT yarns can be identified. The arrangement of the SACNTs is more uniform than that of other types of CNTs (Wang et al., 2020; Wu et al., 2020). Also, there exists abundant interspace among the CNTs, which ensures the passage of water thus facilitating its function as a flow-through electrode. Furthermore, the SACNT film can also function as a membrane that retains foulants through size exclusion. After coated with AC, the resultant SACNT/AC electrode obtained a three-layer structure (Fig. 3C). The bottom PET support layer ensured the overall mechanical strength of the composite electrode. The middle SACNT layer (ultrathin, several microns) and upper AC layer functioned as conductive layers and provided massive space for electrosorption. The surface morphology of the AC layer is same with that of the AC electrode (Fig. 3D).

### 3.2 Superior CDI performance of the SACNT/AC electrode

Both pairs of the AC electrodes and SACNT/AC composite electrodes were separately installed in the CDI system for desalination tests. Fig. 4A and Fig. 4B present the variations of the effluent salt concentrations at different applied voltages (i.e., 0.8, 0.9, 1.0, 1.1, and 1.2 V) in the AC-based and SACNT/AC-based tests, respectively. Both groups of data are typical for a single-pass CDI process (Porada et al., 2013; Suss et al., 2015). At each adsorption stage, an instant concentration decline was observed in the initial period as soon as the voltage was applied, suggesting a rapid salt adsorption process. Several minutes later, the effluent concentration reached a bottom and sharply increased back to its initial level, implying that the electrodes were gradually saturated. In the remaining period of the adsorption stage, the effluent concentration maintained steady. At each desorption stage, an opposite variation trend was observed, demonstrating a standard salt desorption process. Although the overall patterns of the concentration variation for the AC and SACNT/AC were similar, the SACNT/AC-based curves were apparently smoother, implying more stable desalination processes. This could be owing to the existence of the SACNT layer which facilitated the universal connection of the ACs thus promoting the overall stability of the electrode in aqueous environment. Besides, the amplitudes of the adsorption and desorption peaks for the SACNT/AC appeared larger than those for the AC, indicating a possible higher desalination capacity.

The mSACs, ASARs, and SARs for both electrodes were further calculated. As demonstrated in Fig. 4C and

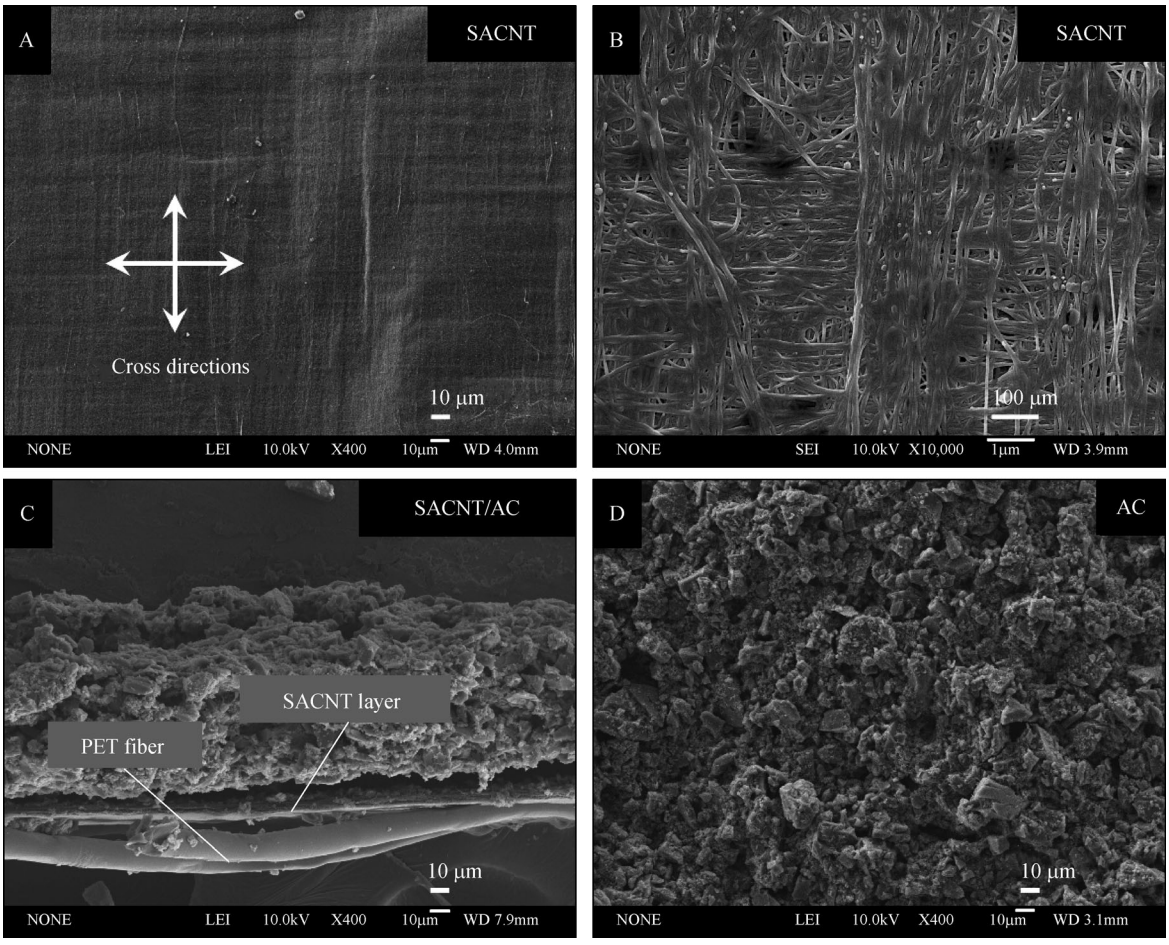


**Fig. 3** SEM views of the (A) surface and (B) local area of the SACNT film, (C) the cross section of the SACNT/AC composite electrode, and (D) the surface of AC electrode.

Fig. 4D, the mSACs and ASARs for both electrodes increased with the applied voltage. This is common for an electrosorption process (Hassanvand et al., 2018; Xu et al., 2019). More importantly, the mSACs and ASARs of the SACNT/AC electrode were approximately two times higher at all the voltages than those of the AC electrode, indicating a superior CDI performance. Additionally, the desalination data at 1.2 V were further calculated to make a comparison of the SARs at different time ($R_{ar}$) between the AC and SACNT/AC electrodes. As shown in Fig. 4E, the SARs for SACNT/AC were significantly higher than those for AC, manifesting a much faster desalination speed. Moreover, the SACNT/AC electrodes also gave rise to a ~26% increase in charge efficiency (Fig. 4F, see the current data in Fig. S2 in Supporting Information), which manifested that the incorporation of the SACNT film reduced the internal consumption of current (Zhang et al., 2018).

The superior desalination performance of the SACNT/AC electrode could be primarily ascribed to two reasons: (i) the SACNTs acted as conductive chains which promoted the overall connection of the ACs and reduced the internal resistance of the electrode; (ii) the ultra-high specific surface area and abundant interior space of the SACNT film provided massive adsorption sites thus leading to dramatically increased adsorption capacity.

### 3.3 Efficient water purification performance via CUF

As discussed in Section 3.1, the SACNT film possessed a potential to be used as a membrane due to its dense and porous structure (Fig. 3). This structure makes it suitable to be used as a filtration electrode in the CUF process. Therefore, the CUF performance of the SACNT/AC electrode for water purification was systematically evaluated in terms of fouling inhibition, foulant retention, and desalination aspects. As demonstrated in Fig. 5A, the TMP increase was observed during every purification stage for all the voltage conditions. This TMP increase indicated the gradual development of membrane fouling which resulted in increased filtration resistance (Ma et al., 2019). However, the TMPs in the tests with an applied voltage (either 0.8, 1.0, or 1.2V) were dramatically lower than those in the control test (i.e., 0 V). As compared with the

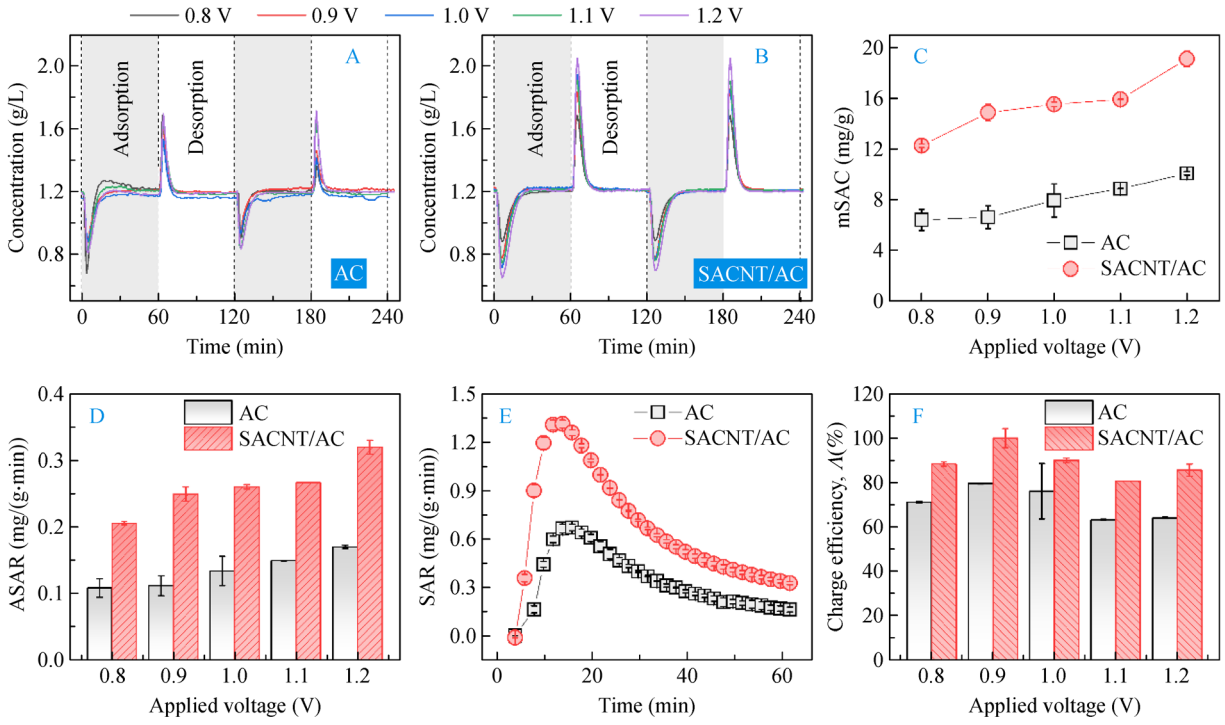


**Fig. 4** Comparison of the CDI performance between the AC and SACNT/AC electrodes at different applied voltages (0.8, 0.9, 1.0, 1.1, and 1.2 V): changes of effluent salt concentration in the CDI tests with the (A) AC electrode pair and (B) the SACNT/AC electrode pair, (C) calculated maximum salt adsorption capacity (mSAC), (D) calculated average salt adsorption rate (ASAR), (E) calculated SAR at different points in time at 1.2 V, and (F) calculated charge efficiency.

control operation (0 V), the applied 0.8, 1.0, and 1.2 V voltages reduced the membrane fouling by ~2.40, ~2.08, and ~2.43 times, respectively, according to the averaged final TMP data at the end of the purification stages (Fig. S3 in Supporting Information). Besides, the average increasing rates of TMP in the 0.8, 1.0, and 1.2 V tests were also roughly two time smaller than that in the 0 V test (Fig. 5B), indicating a much slower development of membrane fouling. This fouling reduction in the CUF process could be mainly ascribed to two fouling mitigation effects: (i) the repulsive effect to the foulants by the electrophoretic force generated by the applied electric field (Huotari et al., 1999; Weigert et al., 1999), and (ii) the indirect effect owing to the changes in solution chemistry (e.g., pH). Specifically, the applied electrical potential brought about an increase of effluent pH, which weakened the adsorption of BSA and HA on the membrane owing to enhanced electrostatic repulsion (Jones and O'Melia, 2000), thus contributing to the reduction of membrane fouling.

In the CUF process, the foulants were expected to be primarily retained by the UF membranes (Fig. 2B). But there also existed a possibility that the SACNT/AC electrodes behind the membrane could contribute to the retention of foulants through size exclusion or physical adsorption, although the equivalent pore size of the electrodes might be too large to retain the foulants. To investigate the foulant-retention capability of the SACNT/AC electrode, two control treatment tests without the UF membranes (resembling the CDI configuration but operated in the one-side CUF mode) were conducted at 0 V and 1.2 V. The TOC concentration of the synthetic influent was measured to be 15.21 mg/L. For both the control tests, the effluent TOC concentrations dropped to around 13 mg/L (Fig. 5C), which should be owing to the physical rejection or adsorption effect by the electrode. Besides, a slight decreasing tendency was observed at every purification stage in the 1.2 V control test, while the corresponding data in the 0 V control test were relatively stable. It implied that the applied electric field might possess a capability to achieve extra retention of foulants via electrosorption or electrophoretic repulsion. In marked contrast, the retention rates in all the normal CUF tests were significantly higher than those in the control tests (Fig. 5D), verifying the dominant role of the UF membranes in foulant retention. Moreover, the 1.2 V voltage brought about a slight increase of retention rate, suggesting the positive effect of the applied electrical power on foulant retention. Whereas, the applied relatively low voltages of 0.8 and 1 V led to decreased retention rates, although these decreases were not significant (with overlapped error bars). We speculate that this phenomenon is related with the spatial orientation change of the foulant molecules in the applied electric field. The applied electric filed might have changed the spatial orientation of the foulants, making it easier for the

foulants to pass through the membrane and electrode. In the meantime, the electric field repulsed the foulants away from the membrane via electrophoretic force. The result of the counterbalance between these two effects determined the overall influence on the foulant retention behavior. At the relatively low voltages (i.e., 0.8 and 1 V), the orientation effect could be the dominating effect, leading to the decreased retention rates. At the higher 1.2 V, the applied electrophoretic force could become the dominating effect, bring about the increased retention rate.

Figure 5E presents the changes of effluent salt concentration during the CUF tests. Similar sharp concave curves were observed at every purification stage. Also, similar to the CDI desalination results (Fig. 4), a larger voltage in the CUF process would lead to a larger SAC (Fig. S4 in Supporting Information) and a higher SAR (Fig. 5F). Moreover, as compared with the control 1.2 V (i.e., no membrane) test, all the CUF tests reached their highest SAR dramatically earlier. This phenomenon could be attributed to the competition of foulants for adsorption sites. In the CUF process, the majority of the foulants were retained by the UF membranes. But in the control test, all the foulants could directly contact with the electrodes, thereby competing with salts for adsorption sites. This

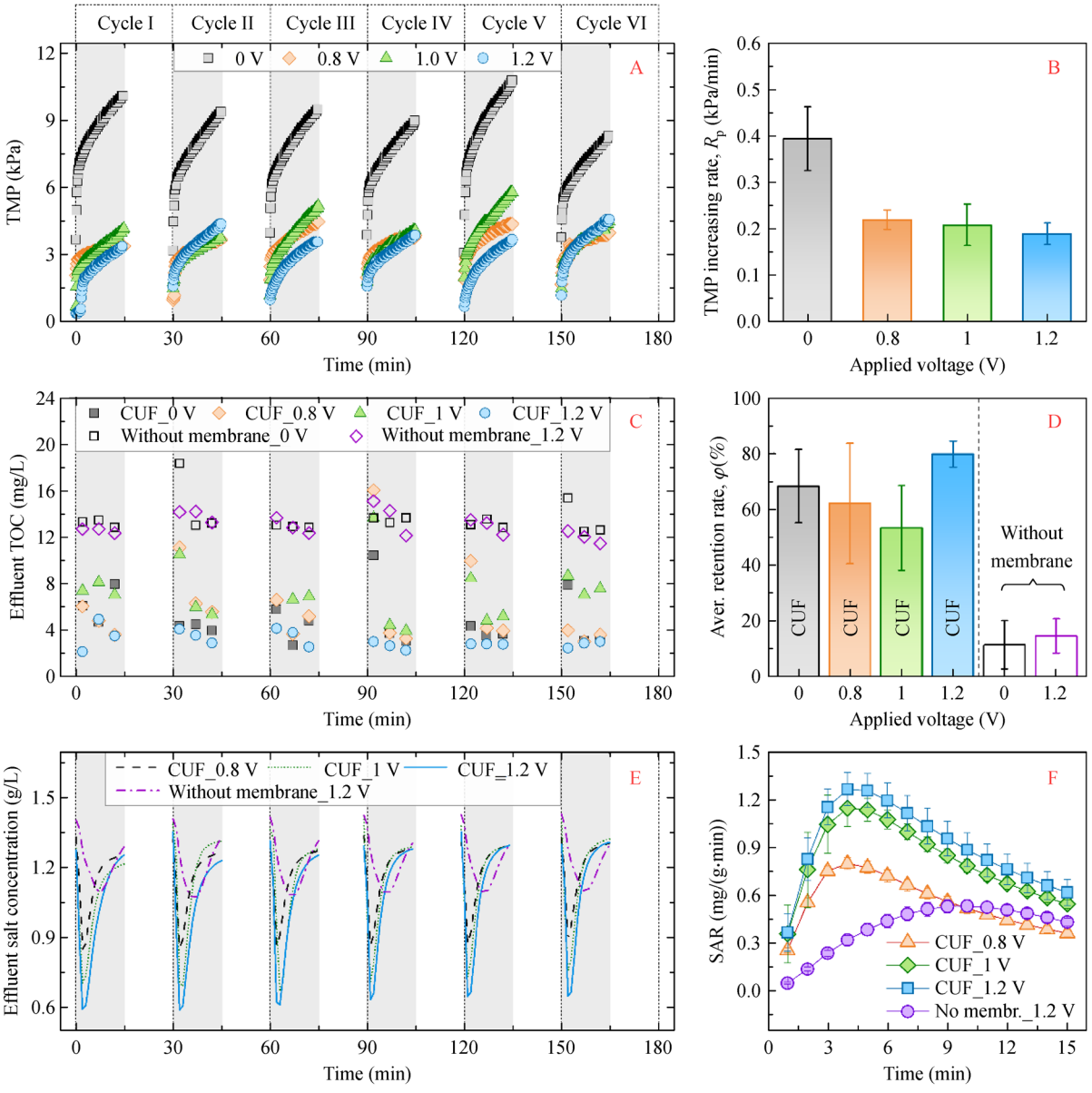


**Fig. 5** Water purification performance via CUF at different voltages of the SACNT/AC electrode: (A) variations of transmembrane pressure (TMP); (B) calculated average TMP increasing rates; (C) variations of effluent total organic carbon (TOC) concentration; (D) calculated average retention rates; (E) variations of effluent salt concentration; and (F) calculated SARs at different time points. The shadow area indicates the purification stage where the external voltage was applied.

competition process not only led to the SAC decrease, but also slowed down the SAR. These results demonstrated the positive effect of the membranes on the desalination process. To sum up, the prepared SACNT/AC electrode achieved a high efficiency of water purification in the CUF process.

Although the prepared SACNT/AC electrode achieved superior desalination performance, it is still less qualified for the CUF application. In the CDI tests, the SACNT/AC electrode reached adsorption saturation within ~30 min. Then a discharging operation was needed to refresh its desalination capability. But the UF process can be continuously operated in days before a backwashing operation. At present, the relatively low capacity of the electrode mismatches the long service capability of the UF process. The oxidation-induced performance deterioration of the electrode also needs to be solved to substantially extend its service life. Future research is needed to further improve the treatment capacity of the electrode.

## 4 Conclusions

A novel SACNT/AC composite electrode was prepared. The desalination capability and water purification performance of the electrode were systematically investigated with a CDI system and a CUF system, respectively. As compared with the control AC electrode, the SACNT/AC composite electrode achieved an approximately 100% increase in both the mSAC and ASAR under all the applied voltage conditions, demonstrating a superior desalination capability. The use of the SACNT/AC electrode also roughly gave rise to a 26% increase in charge efficiency, which would benefit the improvement of the overall treatment efficiency of the CDI process. In the CUF process, the applied 0.8, 1.0, and 1.2 V voltages reduced the membrane fouling by ~2.40, ~2.08, and ~2.43 times (calculated on basis of the final TMP at the end of each purification stage), respectively. The average TMP increasing rates for 0.8, 1.0, and 1.2 V were also roughly two times smaller than that for 0 V, indicating a dramatical fouling inhibition performance. The SACNT/AC electrode also maintained its superior desalination capability in the CUF process, resulting in a high efficiency of water purification.

**Acknowledgements** The authors gratefully acknowledge the financial support from the Beijing Municipal Natural Science Foundation (Nos. 8192030 and L182026), Fundamental Research Funds for the Central Universities (No. 2016ZCQ03), and National Natural Science Foundation of China (Nos. 51608038 and 21975140).

**Electronic Supplementary Material** Supplementary material is available in the online version of this article at https://doi.org/10.1007/s11783-020-1286-1 and is accessible for authorized users.

## References

Caldera U, Breyer C (2017). Learning curve for seawater reverse osmosis desalination plants: Capital cost trend of the past, present, and future. Water Resources Research, 53(12): 10523–10538

Chen G, Ma Z, Xiao K, Wang X, Liang S, Huang X (2019). Hierarchically textured superhydrophilic polyvinylidene fluoride membrane via nanocasting and post-fabrication grafting of surface-tailored silica nanoparticles. Environmental Science. Nano, 6(12): 3579–3589

Choi J, Dorji P, Shon H K, Hong S (2019). Applications of capacitive deionization: Desalination, softening, selective removal, and energy efficiency. Desalination, 449: 118–130

Guo X, Li C, Li C, Wei T, Tong L, Shao H, Zhou Q, Wang L, Liao Y (2019). G-CNTs/PVDF mixed matrix membranes with improved antifouling properties and filtration performance. Frontiers of Environmental Science & Engineering, 13(6): 81

Hassanvand A, Chen G Q, Webley P A, Kentish S E (2018). A comparison of multicomponent electrosorption in capacitive deionization and membrane capacitive deionization. Water Research, 131: 100–109

Hu C Z, Li M Q, Sun J Q, Liu R P, Liu H J, Qu J H (2019). NOM fouling resistance in response to electric field during electro-ultrafiltration: Significance of molecular polarity and weight. Journal of Colloid and Interface Science, 539: 11–18

Huotari H M, Trägårdh G, Huisman I H (1999). Crossflow membrane filtration enhanced by an external DC electric field: A review. Chemical Engineering Research & Design, 77(5): 461–468

Jones K L, O'Melia C R (2000). Protein and humic acid adsorption onto hydrophilic membrane surfaces: Effects of pH and ionic strength. Journal of Membrane Science, 165(1): 31–46

Jung Y T, Narayanan N C, Cheng Y L (2018). Cost comparison of centralized and decentralized wastewater management systems using optimization model. Journal of Environmental Management, 213: 90–97

Kamali M, Suhas D P, Costa M E, Capela I, Aminabhavi T M (2019). Sustainability considerations in membrane-based technologies for industrial effluents treatment. Chemical Engineering Journal, 368: 474–494

Li Y, Chen N, Li Z, Shao H, Qu L (2020). Frontiers of carbon materials as capacitive deionization electrodes. Dalton Transactions (Cambridge, England: 2003), 49, 5006–5014

Liang S, Li M, Cao J, Zuo K, Bian Y, Xiao K, Huang X (2019). Integrated ultrafiltration–capacitive-deionization (UCDI) for enhanced antifouling performance and synchronous removal of organic matter and salts. Separation and Purification Technology, 226: 146–153

Liang S, Xiao K, Wu J, Liang P, Huang X (2014). Mechanism of membrane filterability amelioration via tuning mixed liquor property by pre-ozonation. Journal of Membrane Science, 454: 111–118

Liang S, Xiao K, Zhang S, Ma Z, Lu P, Wang H, Huang X (2018). A facile approach to fabrication of superhydrophilic ultrafiltration membranes with surface-tailored nanoparticles. Separation and Purification Technology, 203: 251–259

Lin S (2020). Energy efficiency of desalination: Fundamental insights from intuitive interpretation. Environmental Science & Technology, 54(1): 76–84

Liu K, Sun Y, Chen L, Feng C, Feng X, Jiang K, Zhao Y, Fan S (2008). Controlled growth of super-aligned carbon nanotube arrays for spinning continuous unidirectional sheets with tunable physical properties. Nano Letters, 8(2): 700–705

Liu K, Sun Y, Liu P, Lin X, Fan S, Jiang K (2011). Cross-stacked superaligned carbon nanotube films for transparent and stretchable conductors. Advanced Functional Materials, 21(14): 2721–2728

Liu L, Lopez E, Dueñas-Osorio L, Stadler L, Xie Y, Alvarez P J J, Li Q (2020). The importance of system configuration for distributed direct potable water reuse. Nature Sustainability,

Lu J Y, Wang X M, Liu H Q, Yu H Q, Li W W (2019). Optimizing operation of municipal wastewater treatment plants in China: The remaining barriers and future implications. Environment International, 129: 273–278

Ma J X, Dai R B, Chen M, Khan S J, Wang Z W (2018). Applications of membrane bioreactors for water reclamation: Micropollutant removal, mechanisms and perspectives. Bioresource Technology, 269: 532–543

Ma Z, Zhang S, Chen G, Xiao K, Li M, Gao Y, Liang S, Huang X (2019). Superhydrophilic and oleophobic membrane functionalized with heterogeneously tailored two-dimensional layered double hydroxide nanosheets for antifouling. Journal of Membrane Science, 577: 165–175

Mekonnen M M, Hoekstra A Y (2016). Four billion people facing severe water scarcity. Science Advances, 2(2): e1500323

Omosa I B, Wang H T, Cheng S P, Li F T (2012). Sustainable tertiary wastewater treatment is required for water resources pollution control in Africa. Environmental Science & Technology, 46(13): 7065–7066

Patel S K, Qin M, Walker W S, Elimelech M (2020). Energy efficiency of electro-driven brackish water desalination: Electrodialysis significantly outperforms membrane capacitive deionization. Environmental Science & Technology, 54(6): 3663–3677

Porada S, Zhao R, Van Der Wal A, Presser V, Biesheuvel P M (2013). Review on the science and technology of water desalination by capacitive deionization. Progress in Materials Science, 58(8): 1388–1442

Suss M E, Porada S, Sun X, Biesheuvel P M, Yoon J, Presser V (2015). Water desalination via capacitive deionization: what is it and what can we expect from it? Energy & Environmental Science, 8(8): 2296–2319

Tay M F, Liu C, Cornelissen E R, Wu B, Chong T H (2018). The feasibility of nanofiltration membrane bioreactor (NF-MBR) + reverse osmosis (RO) process for water reclamation: Comparison with ultrafiltration membrane bioreactor (UF-MBR) + RO process. Water Research, 129: 180–189

Wang L, Lin S H (2019). Theoretical framework for designing a desalination plant based on membrane capacitive deionization. Water Research, 158: 359–369

Wang S, Liang S, Liang P, Zhang X, Sun J, Wu S, Huang X (2015). In-situ combined dual-layer CNT/PVDF membrane for electrically-enhanced fouling resistance. Journal of Membrane Science, 491: 37–44

Wang Y, Lu D, Wang F, Zhang D X, Zhong J, Liang B H, Gui X C, Sun L (2020). A new strategy to prepare carbon nanotube thin film by the combination of top-down and bottom-up approaches. Carbon, 161: 563–569

Weigert T, Altmann J, Ripperger S (1999). Crossflow electrofiltration in pilot scale. Journal of Membrane Science, 159(1–2): 253–262

Wu G, Chen Y, Zhan H, Chen H T, Lin J H, Wang J N, Wan L Q, Huang F R (2020). Ultrathin and flexible carbon nanotube/polymer composite films with excellent mechanical strength and electromagnetic interference shielding. Carbon, 158: 472–480

Xiao K, Liang S, Wang X, Chen C, Huang X (2019). Current state and challenges of full-scale membrane bioreactor applications: A critical review. Bioresource Technology, 271: 473–481

Xu X, Tan H, Wang Z, Wang C, Pan L, Kaneti Y V, Yang T, Yamauchi Y (2019). Extraordinary capacitive deionization performance of highly-ordered mesoporous carbon nano-polyhedra for brackish water desalination. Environmental Science. Nano, 6(3): 981–989

Yan X, Xiao K, Liang S, Lei T, Liang P, Xue T, Yu K, Guan J, Huang X (2015). Hydraulic optimization of membrane bioreactor via baffle modification using computational fluid dynamics. Bioresource Technology, 175: 633–637

Zhang C Y, He D, Ma J X, Tang W W, Waite T D (2018). Faradaic reactions in capacitive deionization (CDI) - problems and possibilities: A review. Water Research, 128: 314–330

Zhang X B, Jiang K L, Feng C, Liu P, Zhang L, Kong J, Zhang T H, Li Q Q, Fan S S (2006). Spinning and processing continuous yarns from 4-inch wafer scale super-aligned carbon nanotube arrays. Advanced Materials, 18(12): 1505–1510

Zhao F, Ma Z, Xiao K, Xiang C, Wang H, Huang X, Liang S (2018). Hierarchically textured superhydrophobic polyvinylidene fluoride membrane fabricated via nanocasting for enhanced membrane distillation performance. Desalination, 443: 228–236

Zhao X, Wu Y, Zhang X, Tong X, Yu T, Wang Y, Ikuno N, Ishii K, Hu H (2019). Ozonation as an efficient pretreatment method to alleviate reverse osmosis membrane fouling caused by complexes of humic acid and calcium ion. Frontiers of Environmental Science & Engineering, 13(4): 55

Zhu X B, Dudchenko A V, Khor C M, He X, Ramon G Z, Jassby D (2018). Field-induced redistribution of surfactants at the oil/water interface reduces membrane fouling on electrically conducting carbon nanotube UF membranes. Environmental Science & Technology, 52(20): 11591–11600

Zhu Z, Peng D, Wang H (2019). Seawater desalination in China: An overview. Journal of Water Reuse and Desalination, 9(2): 115–132